Modeling the dynamics of dendritic actin waves in living cells

Vaibhav Wasnik and Ranjan Mukhopadhyay
Department of Physics, Clark University, Worcester, Massachusetts 01610, USA
(Received 17 October 2013; published 10 November 2014)

The actin cytoskeleton in living cells exhibits a high degree of capacity for dynamic self-organization. Recent experiments have observed propagating actin waves in *Dictyostelium* cells recovering from complete depolymerization of their actin cytoskeleton. The propagation of these waves appear to be dependent on a programmed recruitment of a few proteins that control actin assembly and disassembly. Such waves also arise spontaneously along the plasma membrane of the cell, and it has been suggested that actin waves enable the cell to scan a surface for particles to engulf. Based on known molecular components involved in wave propagation, we present and study a minimal reaction-diffusion model for actin wave production observed in recovering cells.

DOI: 10.1103/PhysRevE.90.052707 PACS number(s): 87.17.Aa

I. INTRODUCTION

The intracellular actin cytoskeleton is a dynamical system where actin filaments treadmill, growing and disassembling continuously, and the actin polymer network undergoes constant and rapid reshaping. Actin dynamics plays a vital role in processes such as cell motility, active cell shape control, generation of cleavage furrow during cell division, and phagocytosis. An understanding of the spatiotemporal dynamics and of self-organization of the cytoskeleton would be of great importance for cellular biophysics. In order to study the the capacity of the intracellular actin system to self-organize, Gunther Gerisch and coworkers studied the temporal evolution of *Dictyostelium* cells treated with the depolymerizing agent Latruculin A [1,2]. In these experiments, the cells were attached to a planar substrate, and, following actin depolymerization, the Latrucilin A was washed away and the subsequent reorganization of actin was studied. The authors reported a defined sequence of patterns: first, the appearance of mobile actin spots, followed by the generation of propagating waves of actin along planar substrate-attached membrane, before the normal organization and polarity of motile cells is restored. Though less frequent and vigorous, similar propagating actin waves have also been observed in normal motile cells. During recovery from depolymerization, in the intermediate wave-forming state, cells exhibit added capability to phagocytose, suggesting a link between the observed actin waves and formation of phagocytic cup in response to curved particles. Moreover, phagocytic cups display a zonal pattern of proteins resembling the pattern of propagating actin waves, suggesting a connection between actin waves and phagocytosis [3].

Bretschneider *et al.* [2] have shown that actin self-organization associated with wave formation involves the ordered recruitment of proteins from the cytoplasmic pool. Three proteins and protein complexes, myosin IB, Arp 2/3 (actin-related protein 2-3 complex) complexes, and coronin, were found to form distinct three-dimensional patterns in association with the actin waves. Myosin IB is enriched at the wave front and close to the plasma membrane, the Arp2/3 complex is distributed throughout the waves, and coronin forms a sloping layer on top of them. CARMIL (capping protein, Arp2/3, and myosin I linker) is also recruited to the waves. The localization of Arp2/3 complexes, which nucleate new actin filaments by branching, suggests the association of propagating waves with dendritic actin. Myosin IB may link the actin network to the membrane, and coronin facilitates disassembly of actin networks. Wave formation does not depend on signals transmitted by heterotrimeric G proteins, nor does their propagation require SCAR (suppressor of G protein-coupled receptors, the cARs), a regulator upstream of the Arp2/3 complex.

Actin waves have been observed in living cells under a variety of other conditions as well. Different types of reaction-diffusion waves of actin have been proposed to determine locomotion and shape of mouse melanoma cells and *Dictyostelium* cells [4]. Actin-based waves of Hem-1 (hematopoietic protein-1) have been discovered in neutrophils and shown to be directed by chemoattractants toward the front of the cells [5]. The waves generated in their study are spontaneously generated in association with the Arp2/3 complex. Related theoretical work has been carried out by several groups, including, for example, in Ref. [6], where the authors proposed a model coupling calcium actin waves with the cell membrane. In Ref. [7], the authors sought to to explain the actin waves in recovering cells in terms of a model where the actin system was treated as an excitable system. In this context, the author of Ref. [8] studied a *in silico* molecular-scale model of stochastic growth of actin which generated traveling waves, though it was not clear whether the model would generate the expanding ringlike wavefronts highlighted in the experimental studies [1]. In Ref. [9], the authors introduced a model of treadmilling actin filaments coupled to the membrane, with waves generated by nucleating proteins that are active when bound to the membrane. While the model is likely to be relevant for a number of scenarios where actin waves are observed, it is most likely not directly applicable to the experiments by Gerisch and coworkers, where the waves are believed to be associated with the assembly and disassembly of dendritic actin. In Ref. [10] a mechanism was proposed in terms of bistability between two structurally distinct forms of the actin network. We will discuss this model under Discussion, noting here only that, to our knowledge, there is no known mechanism for direct interconversion between the two forms; rather, we believe that one form of the network will have to be disassembled for the other form to grow in the same region of space, which has not been adequately

accounted for in the dynamic model proposed by the author. The authors of Ref. [11] have looked at the phenomenon of actin waves by considering the growth of actin filaments in conjunction with signaling proteins. Their model is far more complex than ours with many more parameters. It also incorporates some details of filamentous actin structure but assumes that filaments grow perpendicularly to the substrate and hence that free actin was being added to the filaments close to the membrane. However, in the case of dendritic actin filaments growing at an angle of 70° to each other, it is difficult to understand this addition of free actin to the filaments only close to the membrane. The importance of this assumption for wave production in their model was not discussed. There is also very little discussion about the robustness of their model, the nature of the phase diagrams, and the essential physical mechanism of wave production in their model.

In this paper we develop and study a minimal model for actin wave generation involving known components whose participation in actin propagation has been verified experimentally, while also accounting for dendritic nucleation in relation to actin polymerization. One of our aims is to understand whether the observed dynamics can be accounted for by relatively simple reaction-diffusion type models or whether it will be necessary to invoke more complex models that would account for the detailed dendritic structure of actin. Despite previous theoretical studies, this remains an open question. In our modeling, we refrain from including components that have not been experimentally verified and identify a core motif of the network of chemical reactions that are involved in actin phenomenology. We note, however, that our model is quite robust to addition of new components as we will discuss later, in particular, in the context of myosin IB, which has been hypothesized as being a player in controlling actin polymerization. Our model should help us identify the core underlying physical mechanism for actin wave formation in this system.

II. THE MODEL

The dendritic nucleation model Ref. [12,13] has been proposed to explain the growth dynamics of dendritic actin within cells Fig. 1. External stimuli cause the activation of GTPases [hydrolase enzymes that can bind and hydrolyze guanosine triphosphate (GTP)] and PIP_2 (phosphatidylinositol

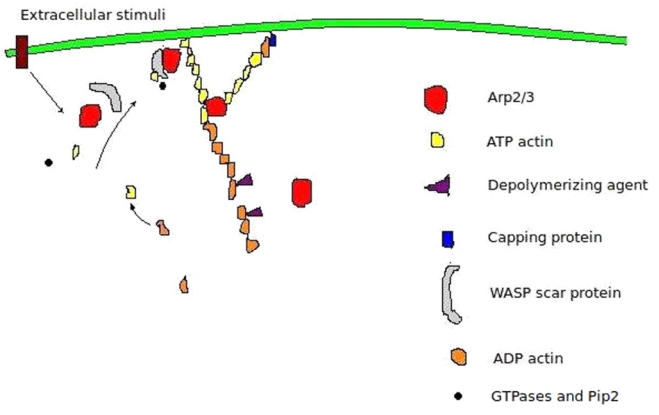

FIG. 1. (Color online) Dendritic nucleation model.

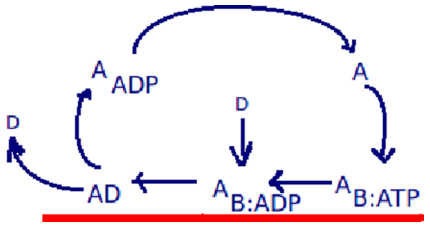

FIG. 2. (Color online) A schemata of the biochemical reactions underlying actin wave generation.

4,5-bisphosphate) signaling proteins. These then activate the WASP-SCAR (WASP is a acronym for Wiskott-Aldrich syndrome protein) cascade which, in turn, activates the Arp2/3 proteins, enabling them to bind to growing actin filaments. The protein complex Arp2/3 is necessary for promoting branching of filamentous actin, thus stabilizing and strengthening dendritic actin structures against stress. Arp2/3 protein units help nucleate new branches of actin filaments at 70° to the mother filament. We expect the growth of dendritic actin to be autocatalytic since in an increase in the number of dendritic actin filaments should increase the number of nucleation events, leading to new branches. The growth of actin filaments is stopped by capping proteins, whose function is to limit the length of filaments and thus to aid the generation of new actin branches at different sites, aiding in strengthening the dendritic structure.

In light of our goal of identifying a base motif of chemical reactions, we simplify the above process in our endeavor to develop a minimal model. In our model, the growth of bound dendritic actin is treated as a simple autocatalyic process, with free ATP-actin (adenosine triphosphate–attached actin) getting converted to bound ATP-actin. Bound ATP-actin hydrolyzes to ADP-actin (adenosine diphosphate–attached actin), which can bind to coronin, which destabilizes dendritic actin; the bound states of ADP-actin with coronin can then result in actin disassembly. Free ADP-actin is converted back to free ATP-actin and the cyclic process continues. In our minimal model, we refrain from explicitly including the effect of the Arp2/3 complex, structural details such as the 70° angle made by actin filaments with their branches, as well as the role of capping proteins. These and other features are indirectly incorporated within the various elements of the model, be they rate constants, the autocatalytic production of bound dendritic actin, and so on. However, we propose that these additional details could be easily incorporated into the model as per future modeling needs. The chemical reactions of our minimal model are shown in Fig. 2, where $A_{B:\mathrm{ATP}}$ represents ATP actin in the bound state and $A_{B:\mathrm{ADP}}$ the ADP actin. A, D, AD, A_{ADP} are the free actin, coronin (which promotes actin disassembly), the actin-coronin bound state, and the free ADP actin, respectively.

The rate equations for the above reactions can be written as

$$\frac{\partial[A_{B:\mathrm{ATP}}]}{\partial t} = \{k_1[A] + k_1{}^B[A]([A_{B:\mathrm{ATP}}] + \alpha_1[A_{B:\mathrm{ADP}}] + \alpha_2[AD])\} \times \left\{\frac{\rho_{\max} - ([A_{B:\mathrm{ATP}}] + [A_{B:\mathrm{ADP}}] + [AD])}{\rho_{\max}}\right\} - k_2[A_{B:\mathrm{ATP}}], \quad (1)$$

$$\frac{\partial[A_{B:\mathrm{ADP}}]}{\partial t} = k_2[A_{B:\mathrm{ATP}}] - k_3[A_{B:\mathrm{ADP}}][D], \quad (2)$$

$$\frac{\partial[AD]}{\partial t} = k_3[A_{B:\mathrm{ADP}}][D] - k_4[AD], \quad (3)$$

$$\frac{\partial[A_{\mathrm{ADP}}]}{\partial t} = \mathcal{D}\nabla^2[A_{\mathrm{ADP}}] + k_4[AD] - k_5[A_{\mathrm{ADP}}], \quad (4)$$

$$\frac{\partial[D]}{\partial t} = \mathcal{D}\nabla^2[D] + +k_4[AD] - k_3[A_{B:\mathrm{ADP}}][D], \quad (5)$$

$$\frac{\partial[A]}{\partial t} = \mathcal{D}\nabla^2[A] + k_5[A_{\mathrm{ADP}}] - \left\{k_1{}^B[A]([A_{B:\mathrm{ATP}}] + \alpha_1[A_{B:\mathrm{ADP}}] + \alpha_2[AD]) + k_1[A]\right\} \times \frac{\rho_{\max} - ([A_{B:\mathrm{ATP}}] + [A_{B:\mathrm{ADP}}] + [AD])}{\rho_{\max}}. \quad (6)$$

Here k_1-k_5 are constants representing reaction rates and $\mathcal{D}$ represents the diffusion constant for ATP, ADP, and coronin. For simplicity, we assume the same diffusion constant for all free molecular species.

The first equation describes the production of bound actin. The first term, $k_1[A](S([A_{B:\mathrm{ATP}}] + \alpha_1[A_{B:\mathrm{ADP}}] + \alpha_2[AD] + s)$, describes the production of bound actin, which depends on the concentration of free actin $[A]$. We find that the constants α_1 and α_2 have to be nonzero for the production of waves. This autocatalytic dependence of the polymerization rate on bound actin is mediated through Arp2/3 for the proposed mechanism. There is also evidence of the role of PIP_3 [phosphatidylinositol 3,4,5-trisphosphate] [3] for wave formation, presumably via coupling of PIP_3 localization to polymerized actin and the regulation of actin polymerization by PIP_3. While we do not explicitly include PIP_3 in our minimal model, PIP_3 will contribute to the autocatalytic process and might play an important role in controlling the values of α_1 and α_2. PIP_3 along with other proteins may bind to both bound ATP-actin as well as bound ADP-actin and may attract free ATP-actin to it. This could explain why actin polymerization depends not only on bound ATP-actin but also on bound ADP-actin. The term $k_1[A]$ inside the bracket was added to ensure that formation of bound actin even in the absence of bound actin to start with. $k_2[A_{B:\mathrm{ATP}}]$ takes into consideration degradation of bound actin. The multiplicative factor $[\rho_{\max} - ([A_{B:\mathrm{ATP}}] + [A_{B:\mathrm{ADP}}] + [AD])]/\rho_{\max}$ is included in order to ensure that the local concentration of the total bound actin does not increase beyond $\rho_{\max}$. In our model, for the purpose of simplicity we do not explicitly incorporate the third dimension (depth) in the model. In the experimental system, the finite thickness of the cell perpendicular to substrate would imply that polymerization of dendritic actin cannot continue arbitrarily and presumably there is a buildup of mechanical stress as the thickness or depth of dendritic actin continues to grow, leading to a reduction in polymerization rate, leading eventually to saturation. The $\rho_{\max}$ term captures this effect.

The $k_2[A_{B:\mathrm{ATP}}]$ in the second equation describes the hydrolysis of bound ATP-actin to bound ADP-actin $[A_{B:\mathrm{ADP}}]$. The binding of bound ADP-actin to the depolymerizing agent is described by the second term $k_3[A_{B:\mathrm{ADP}}][D]$ and also by the first term in the third equation. This bound state destabilizes the actin filament, leading to actin depolymerization and the generation of free ADP-actin $[A_{\mathrm{ADP}}]$ and free destabilizing agent (coronin) $[D]$. The fourth equation gives the evolution of free ADP-actin, with the first term $k_4[AD]$ corresponding to the production of free ADP-actin from bound ADP-actin and coronin, while the final term represents the conversion of free ADP-actin in to free ATP actin. The fifth equation above is the rate equation for coronin and the final equation describing the evolution of the free actin concentration.

III. SIMULATION OF THE EQUATIONS

The equations were simulated in two dimensions using periodic boundary conditions on a square lattice with 100×100 points (see the Supplementary Material [14]). Unfortunately, the values of the rate constants are not known. A different system which nevertheless exhibits somewhat similar behavior in terms of the generation of traveling waves in a reaction-diffusion system is the MinD-MinE system in bacteria; our rate constants are similar to the ones used there [15], which seems reasonable since we do not expect the rate constants to differ by orders of magnitude. In Fig. 3 we show results from simulation of these reaction diffusion equations with the values of the rate constants set at $k_1{}^B = 0.003\ \mu\mathrm{M}^{-1}\,\mathrm{s}^{-1}$, $k_3 = 0.1\ \mu\mathrm{M}^{-1}\,\mathrm{s}^{-1}$, $k_4 = 0.5\ \mathrm{s}^{-1}$, $k_5 = 1\ \mathrm{s}^{-1}$, $k_2 = 20\ \mathrm{s}^{-1}$, $k_1 = 0.05\ \mathrm{s}^{-1}$, $\alpha_1 = 0.6$, $\alpha_2 = 0.3$, and $\rho_{\max} = 2$ mM. The diffusion constants for the free elements were set to be $2.5\ \mu\mathrm{m}^2/\mathrm{s}$. The total concentrations of the actin and depolymerizing agent in the free and bound forms were 1 and 0.3 mM, respectively. We clearly observe wave formation where we find an initial state of homogeneous free actin concentration developing into heterogeneous regions containing mixtures of bound and free actin. These later separated into moving patches of bound actin, ultimately culminating into a pattern of a periodic show of rings of actin growing in size radially outwards (in interpreting the figures, we note that the boundary conditions are periodic in both directions). This pattern was also seen to be a dominating effect in the actin wave experiments by Bretschneider *et al.* [2]. In Fig. 3, 100 units corresponds to a length of 10 μ. The time steps between images in the movie is 0.69 s. The movies skim through $1575 - 1507 = 68$ frames as the waves traverse a distance of 50 units, indicating an average velocity of 0.11 μ m/s, which is consistent with the experimentally observed velocity for wave propagation.

We supplemented these numerical simulations with a linear stability analysis of the system of equations. This involved, first, finding a homogeneous fixed point involving the concentrations of the various molecular components associated with wave propagation elements involved in the process of wave production, for which there exists a fixed point. A linear stability analysis was then carried out about this fixed point. Among the eigenvalues calculated, we identified one eigenvalue with a positive real part. In Fig. 4, we plot the real and imaginary component of this eigenvalue ω as a function of wave number q. The real part governs the growth of a sinusoidal perturbation (with wave number q) about the homogeneous fixed point, while the imaginary part gives us the frequency of oscillation (as a function of q). In Fig. 4 it is seen that for really small values of q we have $\mathrm{Re}\omega > 0$ when $\mathrm{Im}\omega = 0$, implying a Turing-like instability for very small values of q [this feature is more easily visible in Fig. 5(c)] and

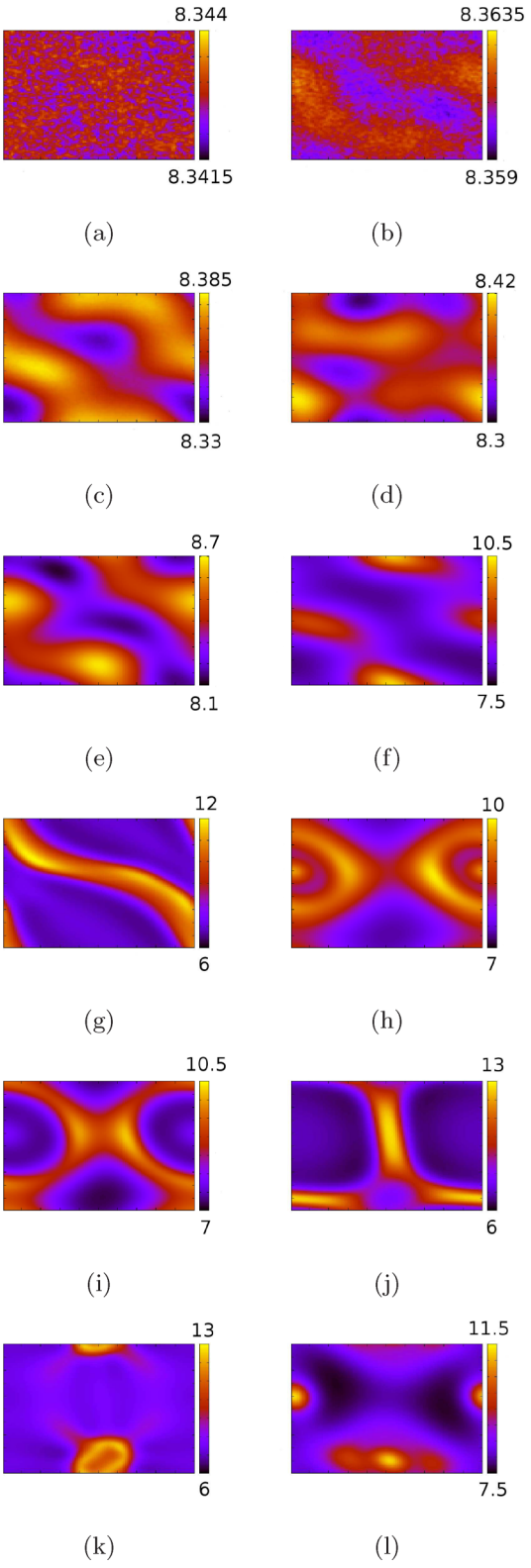

FIG. 3. (Color online) Results of the simulation of Eqs. (1)–(6) in the text. In (a) and (b) we see the homogenous actin breaking up into heterogenous free actin and bound actin. Panels (c)–(f) illustrate these evolving into moving portions of bound actin. Panels (g)–(h) illustrate the formation of rings of bound actin expanding radially outwards (bearing in mind that we implement periodic boundary conditions). These rings die out and reappear periodically, showing similarities to the expanding rings of actin waves seen in the experiments.

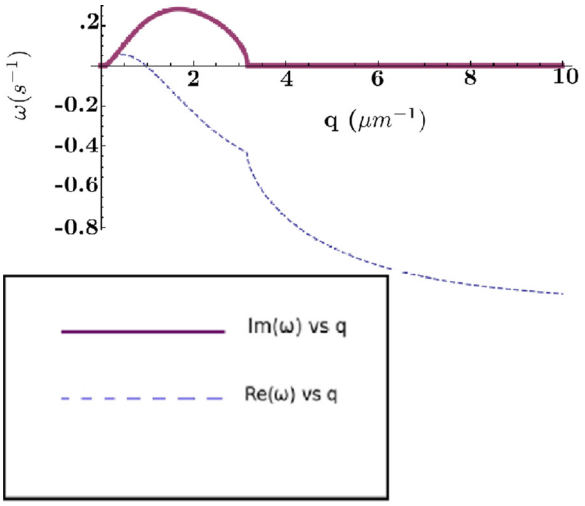

FIG. 4. (Color online) Real and imaginary parts of the eigenvalue of the stability matrix (s^{-1}) with the largest real part plotted against wave number q (μm $^{-1}$).

for a bigger range of q we have Re$\omega > 0$, Im$\omega > 0$, implying a wave like instability.

The maximum slope of the Im(ω)-k graph in Fig. 4 is around 0.1 μm/s, which gives us an estimate of the wave velocity. We find that its value obtained from linear stability analysis agrees with the velocity obtained through an explicit computer simulation of the reaction diffusion equations.

IV. THE PHYSICS OF WAVE PRODUCTION

In order to understand the underlying physical mechanism, we can study the first equation corresponding to the rate of generation of bound ATP-actin. We will seek first to understand why nonzero values of the parameters α_1 and α_2 are essential for wave formation. For that purpose, let us assume that α_1 as well as α_2 are set to zero. If we ignore the $\rho_{\max}$ multiplicative factor, the rate of change of bound ATP-actin, $[A_{B:\mathrm{ATP}}]$, is given by $k_1[A] + k_1^B[A][A_{B:\mathrm{ATP}}] - k_2[A_{B:\mathrm{ATP}}]$. If at time $t = 0$, $[A_{B:\mathrm{ATP}}] = 0$ and all actin exists as free ATP-actin, the level of $[A_{B:\mathrm{ATP}}]$ will continue to build up at a rate dominated by the term $k_1[A]$, while simultaneously the level of $[A]$ will continue to be depleted. Once the level of $[A_{B:\mathrm{ATP}}]$ becomes high enough the rate of change goes to zero, with the level of $[A_{B:\mathrm{ATP}}]$ satisfying the equation $[A_{B:\mathrm{ATP}}] = k_1[A]/(k_2 - k_1[A])$. There is no mechanism in the model to bring the level of $[A_{B:\mathrm{ATP}}]$ back down to lower levels, without which it would be impossible to have stable propagating waves.

In contrast, let us set $\alpha_1 = \alpha_2 = 1$, in which case the rate of change of $[A_{B:\mathrm{ATP}}]$ is given by $k_1[A] + k_1^B[A][A_{B:\mathrm{Total}}] - k_2[A_{B:\mathrm{ATP}}]$, where $A_{B:\mathrm{Total}}$ is the total bound actin both in the ATP and ADP bound forms. Now the autocatalytic component of the growth rate depends on the total bound actin. If we now carry through the previous analysis, as the level of $A_{B:\mathrm{ATP}}$ starts to build up, so does the the level of $A_{B:\mathrm{ADP}}$, which also contributes to the autocatalytic process. Coronin D attaches to $A_{B:\mathrm{ADP}}$ and destabilizes it. This leads to a fall in the level of bound actin, the autocatalytic growth rate for $A_{B:\mathrm{ATP}}$ goes

down and could lead to a decay in the level of $[A_{B:\mathrm{ATP}}]$, thus bringing its level back down.

In order to understand the associated spatiotemporal pattern of localization, consider a propagating wavefront of dendritic actin. At the the front of the wave we have newly generated dendritic ATP-actin. Towards the back of the wave most of the dendritic actin exists as ADP-actin, with some fraction attached to the destabilizing agent D. New actin branches are being polymerized towards the front and dendritic actin continues to be depolymerized (or destabilized) at the back. Once D is released following depolymerization, it diffuses and attaches to adjacent regions of dendritic ADP-actin. Thus the region towards the back of the wave has enhanced concentration of D, while the front of the wave has enhanced growth rate. For a smooth operation of this mechanism, it is essential both that the concentration of D is small enough so a significant fraction of D is in bound form and that there exists a maximum density of dendritic actin characterized by $\rho_{\max}$ that serves to localize growth of dendritic actin to the front of the wave (assuming that the density of dendritic actin in the middle of the wave is sufficiently close to $\rho_{\max}$). It is worth noting that, despite the difference in the details, this mechanism resembles wave formation involving the proteins MinD and MinE in bacteria, with the role of actin resembling that of MinD [15].

In the limit of relatively high levels of free actin and limited amount of coronin (as might be the case for cells recovering after complete depolymerization), we can understand the behavior of the system as a coupled activator-inhibitor system. Here bound actin plays the role of activator while free coronin acts as the inhibitor. Bound actin enhances its own production while also effectively acting as a source for coronin (assuming a significant portion of coronin is bound to dendritic actin). Since it is free coronin that diffuses and not bound actin, in this limit we have a system of local activator and global deactivator, a system that has been studied extensively by Meinhardt and others [16]. However, it is important to note while such a system is expected to exhibit stationary patterns, we do not expect traveling waves. Our intuition is that in order to obtain traveling waves it is important to introduce a delay in the deactivator-induced disassembly. Thus the following two equations might capture the essence of our proposed mechanism in the simplest form (though our equations are strictly not reducible to these in any limit):

$$\begin{aligned} \frac{du}{dt} &= \kappa_1 u(1-u) - \kappa_2 v(t-\tau), \\ \frac{dv}{dt} &= D\nabla^2 v + \kappa_3 u - \kappa_4 v, \end{aligned} \tag{7}$$

where u and v represent dendritic actin and free coronin, respectively, and κ_1, κ_2, κ_3, and κ_4 represent effective rate constants and τ is a delay time so the rate of degradation of actin depends on the level of deactivator at some previous time. In the full model, this time delay is incorporated by the intermediate steps of binding of coronin to dendritic actin and the subsequent disassembly of dendritic actin (there is an additional time delay related to the conversion bound ATP-actin to ADP-actin that is not incorporated in this simplified model). The resulting waves resemble pursuit waves in predator-prey models, with the deactivator (predator) following the the activator (prey), which is consistent with the observed localization profile of coronin. The simplified equations resemble somewhat the equations presented in Ref. [7], though there the constituents u and v were not identified and the authors did not have time delay incorporated into their model and had instead included a form of diffusion for the activator as well, which presumably was crucial for wave formation in their analysis. While their model is reasonable for cortical actin, in this case where the propagating wave corresponds to generation and disassembly of dendritic actin, we believe our model is far more grounded in the underlying biochemistry. Finally, in the limit of lower actin concentration, as is probably the case in normal mobile cells, this simplistic model breaks down and the pattern of actin polymerization following disassembly is governed by diffusion of free actin. In this case, the reduced model is unable to capture even qualitatively the behavior of the system and we need to study the more complete set of reaction-diffusion equations presented earlier.

V. PHASE DIAGRAMS FOR THE MODEL

In the previous section we demonstrated the generation of actin waves for a particular set of parameters and noted that we obtained a value of wave velocity consistent with experimental measurements. Since most of the parameters in our model are effective parameters, we do not know the precise values of these parameters. Thus it would be important to have an understanding of the robustness of wave generation to variations in these parameters. We would also like to characterize systematically the different regimes of behavior exhibited by our model. To do so, we carry out the linear stability analysis as described in the previous section for different values of the parameters. Due to the high dimensionality of parameter space, we study the phase diagrams for variations of two parameters at a time, keeping others fixed at the values $k_1{}^B = 0.003\ \mu\mathrm{M}^{-1}\,\mathrm{s}^{-1}$, $k_3 = 0.093\ \mu\mathrm{M}^{-1}\,\mathrm{s}^{-1}$, $k_4 = 0.5\ \mathrm{s}^{-1}$, $k_5 = 1\ \mathrm{s}^{-1}$, $k_2 = 20\ \mathrm{s}^{-1}$, $k_1 = \times 0.05\ \mathrm{s}^{-1}$, $\alpha_1 = 0.6$, $\alpha_2 = 0.3$, $\rho_{\max} = 2$ mM. The diffusion constants for the free elements were set to be $2.5\ \mu\mathrm{m}^2/\mathrm{s}$. The total concentrations of the actin and coronin in the free and bound forms were 1 and 0.3 mM, respectively. For each value of the two parameters in question the wave number was varied over a particular interval. An instability about the homogeneous state was identified by checking if the real part of any eigenvalue was positive. If the interval of the wave number, q, over which the real part of the leading eigenvalue was positive, the imaginary part being zero for at least some subrange of q implied the occurrence of a Turing instability and while the imaginary part being nonzero implied the existence of a wave like instability. Thus we look for four possibilities: a homogeneous stable steady state with no instabilities, wavelike instability, Turing instability, and mixed Turing wave-like instability. For wavelike instability, we expect stable propagating waves, for Turing instability we expect formation of stationary patterns consisting of regions with different chemical concentrations, and for the case of mixed instability we expect traveling waves for some set of

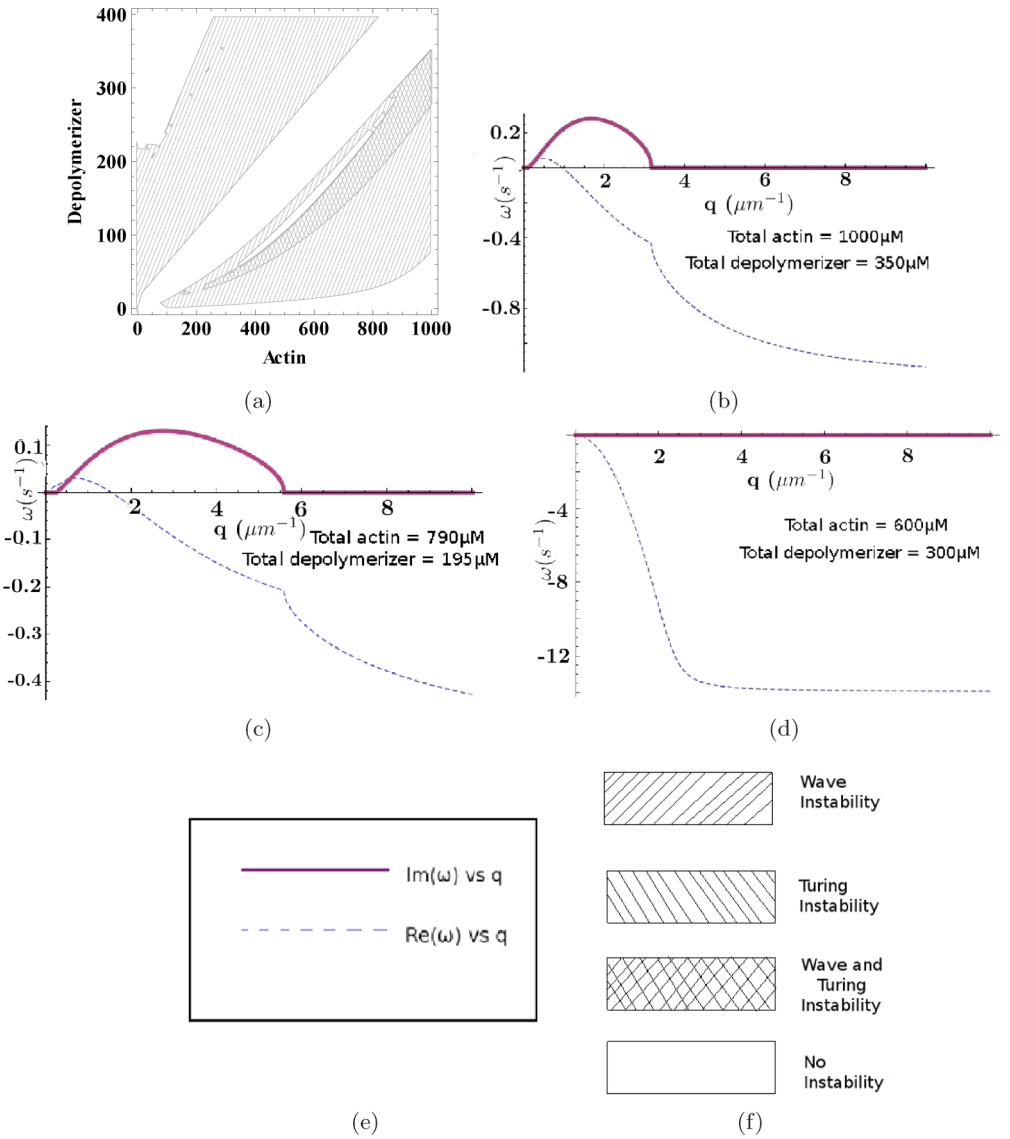

FIG. 5. (Color online) (a) Region plot showing the regions of Turing and wave instabilities for various values of the total actin concentration and total destabilizing agent concentration. (b) Real and imaginary parts of the eigenvalue with the largest real component (s^{-1}) plotted against q (μm^{-1}) for 1000 μM of total actin concentration and 350 μM total destabilizing agent (coronin) concentration, clearly showing the presence of a wavelike instability. (c) Real and imaginary parts of the corresponding eigenvalue with the largest real component (s^{-1}) plotted against q (μm^{-1}) for 790 μM of total actin concentration and 195 μM total destabilizing agent concentration, clearly showing the presence of a Turing as well as a wave instability. (d) Real and imaginary parts of the stability matrix with the largest real component (s^{-1}) plotted against q (μm^{-1}) for 600 μM of total actin concentration and 300 μM total coronin concentration showing the lack of instabilities.

wavelengths coexisting with stationary patterns for a different range of wave numbers.

Let us look at Fig. 5(a). The total actin concentration is plotted along the x axis and the total coronin concentration $[D]$ along the y axis. The shaded region with positively sloped hashed lines correspond to the wave instability and the regions shaded by negative sloped lines correspond to Turing instabilities. We do not find pure Turing instability for any actin or coronin concentration (for this set of parameters) but do find both regions of wave and mixed instability; however, the phase space corresponding to wavelike is far larger than that for mixed instability. The regions of no instability are the white regions. There are three regions that can be identified with no instability: (1) very low coronin concentrations, (2) low actin, very high coronin concentrations, and (3) similar actin and coronin concentrations. The wavelike instabilities lie between these three regions. Regions (1) and (2) correspond to insufficient concentrations of coronin and actin, respectively, to destabilize the homogeneous state. In region (3) the reason the homogeneous state is stable is more subtle and corresponds to cancellations of unstable behaviors. Moreover, we note that, for a given coronin concentration, there are two regions of wavelike instability, one for lower actin concentrations and one for higher actin concentrations, and speculate that the region for higher actin concentration might correspond to recovering cells following actin depolymerization, while the other region might correspond to cells under physiological conditions (since it is expected that there is relative low

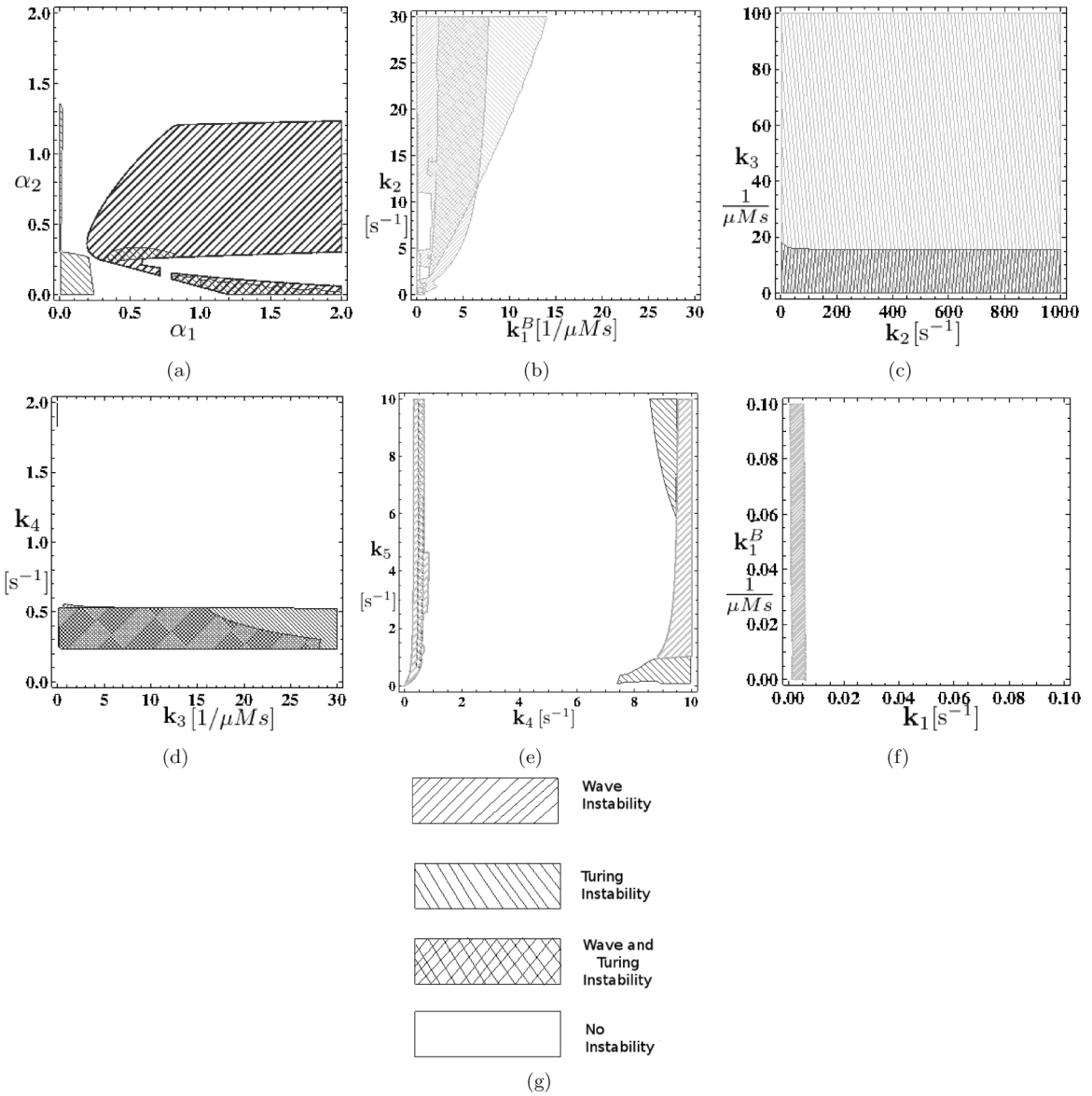

FIG. 6. The phase-space diagrams showing the regions of wave and Turing instabilities as well as the regions where the homogeneous steady state is stable for variations of different parameters in the model.

concentrations of free actin not directly associated with the cytoskeleton in normal cells).

Next, lets look at Fig. 6(a), which plots variations of α_1 versus α_2 along the x and y axes, respectively. We note that there is a larger region for wavelike instability than for Turing instability. However, unlike the previous case, there are regions with only Turing instabilities. It seems that very small values of α_1 and α_2 favor Turing instabilities over wave instabilities. This agrees with our previous discussion of the importance of time delay for wave generation.

For variations in k_1 and k_1^B, we would like to highlight that the value of k_1 has to be relatively small in order to get traveling waves as for larger values of k_1 the homogeneous state is stable. The presence of traveling waves seems to be relatively robust, however, to variations in k_1^B.

Next, let us consider Fig. 6(b) with values of ${k_1}^B$ plotted along the x axis and k_2 along the y axis. We find a state of Turing phase separation at high values of k_1^B, noting, however, that the values of k_1^B has to be orders of magnitude larger than our chosen value in order to get such a state. For the appropriate window of k_1^B, the existence of the traveling wave instability appears to be robust to variations in k_2. However, we note the appearances of small patches at small values of k_1^B and regions of k_2 where no instabilities occur. We also note certain regions which are bounded by regions of pure wave and Turing instabilities which have both Turing and wave instabilities.

When we analyze the variations over k_2 versus k_3 in Fig. 6(c), with k_2 plotted along the x axis and k_3 along the y axis, we find that Turing instabilities are possible over the entire phase space while wave patterns co-occur for k_3 below a particular critical value.

Next, let us consider the variations of k_3 and k_4 as seen in Fig. 6(d), with k_3 plotted along the x axis and k_4 along the y axis. We see a band in the k_3 versus k_4 phase space where the instabilities occur. Turing instabilities occur over a larger region compared to the wave instabilities which always occur

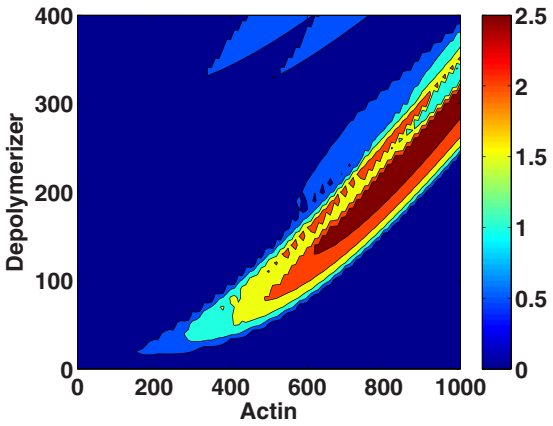

FIG. 7. (Color online) Speed variations of bound actin with changing actin and depolymerizing agent concentrations. The speed is in the unit of μm/s while the concentrations are in units of μM.

as mixed Turing-wave like instability. We note the absence of instability for larger values of k_4, leading us to the conclusion that rapidity of disassembly destroys the wave instability, in agreement with our discussion of the importance of time delay in the previous section

In the final subfigure with variations of k_4 versus k_5 as seen in Fig. 6(e), with k_4 plotted along the x axis and k_5 along the y axis, we note that most of the phase space is about stable regions, implying that k_4, which is the rate of degradation of bound actin, has to be finely tuned in order to get any instabilities.

To sum up, for instability generation, we notice particular sensitivity to the parameters k_1, which is the background rate for bound actin formation, and k_4, which is the rate of disassembly of dendritic actin bound to coronin. This highlights the importance of auto-activation compared to the background dendritic actin assembly rate, as well as the importance of time delay in coronin-induced actin disassembly.

VI. SPEED VARIATIONS

Figure 7 shows the variation of speed of actin waves with variations in actin and depolymerizer concentrations. Comparing to Fig. 5(a), we can see that the wave speed is higher in regions with mixed wave and Turing instabilities compared to regions with pure wave instabilities. Higher speeds would point to faster reaction times by the cell. Turing patterns, on the other hand, would point to constructs of bound actin within the cell that could be utilized for cell processes. Hence a faster reaction time in conjunction with formation of cell constructs within the cell point to a maximizing of a cell's survival response after being subject to a depolymerization of its cytoskeleton.

VII. DISCUSSION

In this paper, we have developed and studied a basic minimal model based on known ingredients in order to understand actin wave generation in recovering *Dictyostelium* cells. The model clearly does not capture the complexity of the *in vivo* system, but we believe it captures the essential physical mechanism of wave generation. Our hope is that the model presented here would provide the foundation for more detailed modeling studies. A more detailed study might include structural details of dendritic actin and finer details of the mechanism by which the coronin destabilizes dendritic actin. Coronin might be far more efficient in destabilizing actin than our model suggests, and thus our proposed regime might actually correspond to significantly lower concentrations of coronin. Moreover, we have not included explicitly the effects of myosin IB and PIP_3 in our model, both of which we believe contribute to the autocatalytic step.

As a first step, let us consider including the role of myosin IB in our model. Myosin IB does seem to be involved in aiding the production of bound actin [17–19]. How it actually does this is not entirely clear. However, we see that we can easily augment the motif of chemical reactions in our model to take into consideration the possible role that myosin IB plays in the autocatalysis of bound actin formation, through the chemical reactions below. [MY] and [MY$_F$] correspond to the concentrations of the bound and free myosin IB. The values for the parameters from the minimal model described in the previous sections just carry over to the model with addition of myosin. The extra equations for [MY] and [MY$_F$] introduce new parameters whose values are chosen as $k_{\rm on} = 1$ and $k_{\rm off} = 1$. Also, $\rho_{\rm max}$ is chosen to be 70 000 μM. The waves produced through the simulation of these equations are illustrated in the Supplementary Material [14]. The changed equations are shown below.

$$\begin{aligned}
\frac{\partial[A_{B:\mathrm{ATP}}]}{\partial t} &= \left\{k_1{}^B[\mathrm{MY}][A]([A_{B:\mathrm{ATP}}] + \alpha_1[A_{B:\mathrm{ADP}}]\right. \\
&\quad \left. + \alpha_2[AD]) + k_1[\mathrm{MY}][A]\right\} \\
&\quad \times \frac{\rho_{\rm max} - ([A_{B:\mathrm{ATP}}] + [A_{B:\mathrm{ADP}}] + [AD])}{\rho_{\rm max}} \\
&\quad - k_2[A_{B:\mathrm{ATP}}] \\
\frac{\partial[A]}{\partial t} &= \mathcal{D}\nabla^2[D] + k_5[A_{\mathrm{ADP}}] - \left\{k_1{}^B[\mathrm{MY}][A]([A_{B:\mathrm{ATP}}]\right. \\
&\quad \left. + \alpha_1[A_{B:\mathrm{ADP}}] + \alpha_2[AD]) + k_1[\mathrm{MY}][A]\right\} \\
&\quad \times \frac{\rho_{\rm max} - ([A_{B:\mathrm{ATP}}] + [A_{B:\mathrm{ADP}}] + [AD])}{\rho_{\rm max}} \\
\frac{\partial[\mathrm{MY}]}{\partial t} &= -k_{\rm off}[\mathrm{MY}] + k_{\rm on}[AB][\mathrm{MY}_F] \\
\frac{\partial[\mathrm{MY}_F]}{\partial t} &= \mathcal{D}\nabla^2[\mathrm{MY}_F] + k_{\rm off}[\mathrm{MY}] - k_{\rm on}[AB][\mathrm{MY}_F].
\end{aligned} \tag{8}$$

As a further comment, let us revisit the mechanism proposed in Ref. [10] in terms of a sharp transition between bundled actin and dendritic actin, with dendritic actin present in the interior of the wave and bundled actin existing exterior to the wave. In the absence of a known mechanism for direct interconversion between bundled actin and dendritic actin, we do not find particular justification for a dynamical model as proposed in Ref. [10]. Instead, it seems reasonable to assume free actin can either polymerize to form bundled actin or dendritic actin, both drawing from the same pool of free actin, which could be incorporated in an extension of our proposed

model with two sets of coupled reaction-diffusion type models feeding from the same pool of free actin, the first corresponding to dendritic actin as proposed here and a second corresponding to formation and disassembly of bundled actin. We will not attempt such a construction in this paper, nevertheless noting that our model of dendritic actin can, by itself, produce a relatively sharp edge for the dendritic actin wavefront, as observed *in vivo*, without the need for a direct transition between the two forms of bound actin.

VIII. CONCLUSIONS

The actin cytoskeleton is a prime player in cell locomotion and in determining cell shape. Understanding the various components of actin phenomenology inside cells is crucial in our understanding of cell biology. From a systems viewpoint, we treat the cell as a system whose components function in concert and where this functioning can be understood at varying degree of complexity. In this work we are guided by the goal of identifying a critical motif of chemical reactions underlying actin wave formation in recovering *Dictyostelium* cells in order to uncover the essential physical mechanism. We concentrate on the temporal evolution of actin in a cell with its bound actin depolymerized. The core system associated with wave formation in cells recovering from complete depolymerization also appears to be involved in the formation of phagocytic cups involved in phagocytosis and important for nutrient intake [3]. In this paper, we presented a minimalistic reaction diffusion model as a motif in actin phenomenology to explain this phenomenon of production of actin waves. We identified the physical mechanism responsible for wave production. The simulation of the reaction diffusion equations showed the explicit formation of growing rings of bound actin as seen in experiments. The reaction diffusion system of equations utilized only experimentally known aspects of actin phenomenology. The formation of actin waves in our model was not constrained with the addition of a large number of parameters that had to be specifically tweaked in order to produce wavelike behavior. We found that the base motif of chemical reactions was robust to additions of other components which we explicitly illustrated by inclusion of myosin IB in to our model

Our model suggests that bound ADP-actin as well as the ADP-actin and the disassembling agent bound state need to contribute to the autocatalytic process of production of bound ATP-actin for the production of stable actin waves. We note also that the formation of instabilities in general is very sensitive to the background rate of bound actin formation and the rate of bound actin degradation, clarifying the role of these processes for wave generation.

As far as experimental predictions go, we note that the parameters that we could change in the model experimentally are the total actin and total coronin concentrations. If the concentrations of the actin and coronin were comparable, neither wavelike nor Turing instabilites were observed in our modeling studies. A similar lack of instabilities was also seen when the ratio of the actin versus the coronin concentrations was “extremely” high or “extremely” low. It was in the “intermediate” regions of low actin and high coronin and high coronin and low actin concentrations that instabilities were seen. We also noted the sensitivity of wave generation to the rate constants k_3 and k_4 related, respectively, to coronin binding to actin and the subsequent disassembly of dendritic actin, where wave generation would be disrupted for higher values of the rate constants which might be experimentally testable by using mutant forms of coronin.

In future work, we plan to couple our model to membrane mechanics in order to elucidate the relation to phagocytosis.

ACKNOWLEDGMENTS

We thank Buddhapriya Chakroborty, Denis Larochelle, and Ned S. Wingreen for helpful discussions and acknowledge funding from NSF Grant No. PHY08-48550. R.M. also acknowledges support from NIH through Grant No. R01 GM082938.

[1] G. Gerisch, T. Bretschneider, A. Muller-Taubenberger, E. Simmeth, and M. Ecke, Biophys. J. **87**, 3493 (2004).
[2] T. Bretschneider, K. Anderson, M. Ecke, A. M. Muller-Taubenberger, B. Schroth-Diez, H. C. Ishikawa-Ankerhold, and G. Gerisch, Biophys. J. **96**, 2888 (2009).
[3] G. Gerisch, M. Ecke, B. Schroth-Diez, S. Gerwig, U. Engel, L. Maddera, and M. Clarke, PMC Biophys. **3**, 7 (2010).
[4] M. G. Vicker, Exp. Cell Res. **275**, 54 (2002)
[5] O. D. Weiner, W. A. Marganski, L. F. Wu, S. J. Altschuler, and M. W. Kirschner, PLoS Biol. **5**, e221 (2007).
[6] A. Veksler and N. S. Gov, Biophys. J. **97**, 1558 (2009).
[7] S. Whitelam, T. Bretschneider, and N. J. Burroughs, Phys. Rev. Lett **102**, 198103 (2009).
[8] A. E. Carlsson, Phys. Rev. Lett **104**, 228102 (2010).
[9] K. Doubrovinski and K. Kruse, Europhys. Lett. **83**, 18003 (2008).
[10] C. Beta, PMC Biophys. **3**, 12 (2010).
[11] V. Khamviwath, J. Hu, and H. G. Othmer, PLoS ONE **8**, e64272 (2013).
[12] T. D. Pollard, L. Blanchoin, and R. D. Mullins, Annu. Rev. Biophys. Biomol. Struct. **29**, 545 (2000).
[13] T. D. Pollard, Nature **422**, 741 (2003).
[14] See Supplemental Material at http://link.aps.org/supplemental/10.1103/PhysRevE.90.052707 for the actin myosin waves simulation.
[15] K. C. Huang, Y. Meir, and N. S. Wingreen, Proc. Natl. Acad. Sci. USA **100**, 12724 (2003).
[16] H. Meinhardt, *Models of Biological Pattern Formation* (Academic Press, New York, 1982).
[17] I. M. Geli, R. Lombardi, B. Schmelzl, and H. Riezman, The EMBO J. **19**, 4281 (2000).
[18] Y. Fukui, Nature **341**, 328 (1989).
[19] K. D. Novak, M. D. Peterson, M. C. Reedy, and M. A. Titus, J. Cell Biol. **131**, 1205 (1995).